Braunschweig J, Klier C, Schröder C, Handel M, Bosch J, Totsche KU & Meckenstock RU (2014) Citrate influences microbial Fe hydroxide reduction via a dissolution-disaggregation mechanism, *Geochimica et Cosmochimica Acta*, 139, pp. 434-446.

This is the peer reviewed version of this article

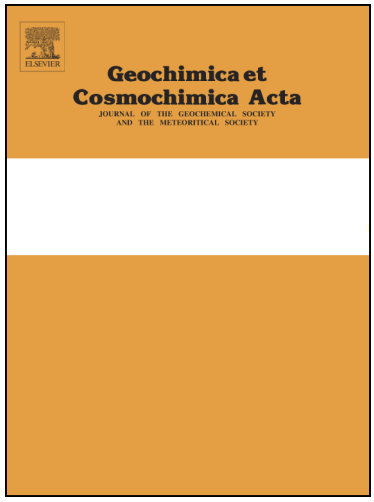

Citrate influences microbial Fe hydroxide reduction via a dissolution-disaggregation mechanism

Juliane Braunschweig, Christine Klier, Christian Schröder, Matthias Händel, Julian Bosch, Kai U. Totsche, Rainer U. Meckenstock

PII: S0016-7037(14)00335-4
DOI: http://dx.doi.org/10.1016/j.gca.2014.05.006
Reference: GCA 8808

To appear in: *Geochimica et Cosmochimica Acta*

Received Date: 20 December 2013
Accepted Date: 3 May 2014

Please cite this article as: Braunschweig, J., Klier, C., Schröder, C., Händel, M., Bosch, J., Totsche, K.U., Meckenstock, R.U., Citrate influences microbial Fe hydroxide reduction via a dissolution-disaggregation mechanism, *Geochimica et Cosmochimica Acta* (2014), doi: http://dx.doi.org/10.1016/j.gca.2014.05.006

Citrate influences microbial Fe hydroxide reduction via a dissolution-disaggregation mechanism

Juliane Braunschweig[a], Christine Klier[a], Christian Schröder[b,c], Matthias Händel[d], Julian Bosch[a], Kai U. Totsche[d], Rainer U. Meckenstock[a, *]

[a] *Institute of Groundwater Ecology, Helmholtz Zentrum München – German Research Center for Environmental Health, D-85764 Neuherberg, Germany*

[b] *Center for Applied Geosciences, Eberhard Karls Universität Tübingen, D-72074 Tübingen, Germany*

[c] *Department of Hydrology, Universität Bayreuth, D-95440 Bayreuth, Germany*

[d] *Lehrstuhl für Hydrogeologie, Institut für Geowissenschaften, Friedrich-Schiller-Universität Jena, D-07749 Jena, Germany*

[*] **Corresponding author. Rainer U. Meckenstock; Tel.: +49 89 3187 2561; fax: +49 89 3187 3361**

E-mail addresses:
juliane.braunschweig@googlemail.com (J. Braunschweig)
christine.klier@helmholtz-muenchen.de (C. Klier)
christian.schroeder@ifg.uni-tuebingen.de (C. Schroeder)
matthias.haendel@uni-jena.de (M. Händel)
kai.totsche@uni-jena.de (K. U. Totsche)
julian.bosch@helmholtz-muenchen.de (J. Bosch)
rainer.meckenstock@helmholtz-muenchen.de (R. U. Meckenstock)

Abstract

Microbial reduction of ferric iron is partly dependent on Fe hydroxide particle size: nanosized Fe hydroxides greatly exceed the bioavailability of their counterparts larger than 1 µm. Citrate as a low molecular weight organic acid can likewise stabilize colloidal suspensions against aggregation by electrostatic repulsion but also increase Fe bioavailability by enhancing Fe hydroxide solubility. The aim of this study was to see whether adsorption of citrate onto surfaces of large ferrihydrite aggregates results in the formation of a stable colloidal suspension by electrostatic repulsion and how this effect influences microbial Fe reduction. Furthermore, we wanted to discriminate between citrate-mediated colloid stabilization out of larger aggregates and ferrihydrite dissolution and their influence on microbial Fe hydroxide reduction. Dissolution kinetics of ferrihydrite aggregates induced by different concentrations of citrate and humic acids were compared to microbial reduction kinetics with *Geobacter sulfurreducens*. Dynamic light scattering results showed the formation of a stable colloidal suspension and colloids with hydrodynamic diameters of 69 (± 37) to 165 (± 65) nm for molar citrate:Fe ratios of 0.1 to 0.5 and partial dissolution of ferrihydrite at citrate:Fe ratios ≥ 0.1. No dissolution or colloid stabilization was detected in the presence of humic acids. Adsorption of citrate, necessary for dissolution, reversed the surface charge and led to electrostatic repulsion between sub-aggregates of ferrihydrite and colloid stabilization when the citrate:Fe ratio was above a critical value (≤ 0.1). Lower ratios resulted in stronger ferrihydrite aggregation instead of formation of a stable colloidal suspension, owing to neutralization of the positive surface charge. At the same time, microbial ferrihydrite reduction increased from 0.029 to 0.184 mM h^{-1} indicating that colloids stabilized by citrate addition enhanced microbial Fe reduction.

Modelling of abiotic dissolution kinetics revealed that colloid stabilization was most pronounced at citrate:Fe ratios of 0.1 – 0.5, whereas higher ratios led to enhanced dissolution of both colloidal and larger aggregated fractions. Mathematical simulation of the microbial reduction kinetics under consideration of partial dissolution and colloid stabilization showed that the bioaccessibility increases in the order large aggregates < stable colloids < Fe-citrate.

These findings indicate that much of the organic acid driven mobilization of Fe oxy(hydr)oxides is most likely due to colloid formation and stabilization rather than solubilisation.

Keywords: *Geobacter*; citrate; ligand; nanoparticles; electrostatic stabilization; mineral dissolution; mathematical modelling

1 Introduction

Iron (Fe) hydroxides are highly abundant in soils and sediments and play an important role in microbial redox processes (Weber et al., 2006). Redox cycling of Fe contributes significantly to carbon and energy flows in the subsurface (Roden, 2012), and both oxidation and reduction of Fe are coupled to many other biogeochemical reactions (Weber et al., 2006). A limiting factor for microbial Fe reduction is the low reactivity of macroparticulate Fe hydroxides, i.e. particles larger than 1 µm, due to their high crystallinity and low solubility at circumneutral pH. Different studies have shown that the reactivity of nanoparticulate Fe hydroxides increases with decreasing particle size (Madden and Hochella, 2005; Madden et al., 2006; Yan et al., 2008) and exceeds the reactivity of micrometer-sized Fe hydroxide particles (Bosch et al., 2010; Waychunas et al., 2005) most likely due to their high surface area. Roden (Roden, 2003) observed a strong dependency of both biotic and abiotic reactivity on the specific surface areas of the Fe hydroxides. Furthermore, nanoparticles exhibit unique material properties (Hochella et al., 2008; Waychunas et al., 2005) which can cause reactivities beyond surface related effects. Bosch et al. (Bosch et al., 2010) showed ~80-100% reduction of colloidal Fe hydroxides by *G. sulfurreducens* irrespective of individual crystallinity.

Another way of increasing the microbial bioavailability of Fe hydroxides is by electron shuttling e.g. by humic acids (Amstaetter et al., 2012; Piepenbrock et al., 2014), or by ligand-induced dissolution. Among the low molecular weight organic acids, citric acid is the most important complex forming compound in O and E horizons in podzol soils (van Hees and Lundström, 2000). Citrate adsorbs immediately to the soil matrix of the A horizon (Hashimoto, 2007; Jones and Brassington, 1998; Lackovic et al., 2003; Oburger et al., 2011) and therefore enhances the solubility of pedogenic minerals (Miller et al., 1986). Complexes of organic acids with Fe and Al are transported downwards, leading to an eluvial horizon, followed by reprecipitation of sesquioxides in deeper horizons (Anderson et al., 1982; Buurman and Jongmans, 2005; de Corninck, 1980; do Nascimento et al., 2004; Lundström, 1994; Lundström et al., 2000; van Hees et al., 2000). Although colloids of nanosized Fe hydroxides with organic coatings were detected in soil solutions (Allard et al., 2011; Riise et al., 2000), organic complexes of Fe and Al are assumed to be the most important mobile fraction, causing metal delocalization.

Ligand-induced dissolution of Fe hydroxides is a process that depends on surface concentrations of adsorbed ligands (Furrer and Stumm, 1986) and on the solution saturation state (Kraemer and Hering, 1997). The mechanism proposed by Furrer and Stumm (Furrer and Stumm, 1986) includes four reaction steps: first, the surface metal centers are coordinated via a ligand exchange reaction. Second, the formation of a kinetically labile Fe surface species occurs. Then, the slow and rate-determining detachment of the coordinated metal centers takes place and finally the mineral surface is protonated.

Organic ligands like citrate have a strong impact on stability and mobility of colloidal or nanoparticulate Fe hydroxides. Colloids are particles or aggregates with diameters between 1 nm and 1 µm (IUPAC, 1997). Electrostatic stabilization caused by adsorbed citrate stabilizes colloidal suspensions against aggregation (Mikutta et al., 2010) and helps to form small particles from larger aggregates (Stumm and Furrer, 1987). The stability of a colloidal suspension in turn has a strong impact on the reactivity of Fe hydroxides caused by the higher specific surface area compared to large aggregates. Thus, the question arises how low-molecular weight organic acid related dissolution, disintegration, and electrostatic stabilization may impact ferrihydrite reactivity.

Therefore, the aim of this work was to investigate microbial ferrihydrite reduction with respect to mineral dissolution and colloid stabilization by electrostatic repulsion forces between citrate-coated sub-units of ferrihydrite. In particular, we studied the microbial accessibility of ferrihydrite within a stable colloidal suspension compared to larger, strongly aggregated ferrihydrite and dissolved Fe species.

2 Materials and methods

2.1 Synthesis of ferrihydrite aggregates

Two-line ferrihydrite aggregates were synthesized according to Lovley and Phillips (Lovley and Phillips, 1986). Five hundred mL of a 0.4 M $FeCl_3$ solution (reagent grade, Sigma-Aldrich, Germany) were titrated to pH 7.0 with 1 M NaOH (p.a., A.C.S. reagent, Sigma-Aldrich). After precipitation of ferrihydrite, the supernatant was discarded. To remove remaining ions from the preparation, the precipitate was washed with MilliQ water (Conductivity = 18.2 µS/cm, 4 ppb TOC, MilliporeElix + Milli-Q Advantage 10A, USA) for at least 5 times. Hydrodynamic

diameters (as measured by Dynamic Light Scattering, see section 2.8) of the obtained ferrihydrite aggregates were 4,200 ± 2,700 nm.

Possible recrystallization of ferrihydrite in the presence of citrate to a ferromagnetic form as described recently (Barrón and Torrent, 2002; Barrón et al., 2003; Michel et al., 2010) was tested by adding 24 mL of 0.05 M Na_3-citrate (puriss., Riedel-de Haën, Germany) to 30 mL of 2-line ferrihydrite (0.25 mol L^{-1}). The suspension was shaken in the dark at 30 °C for seven days. To separate the ferrihydrite from the supernatant, the sample was centrifuged for 20 min with 3,000 x g at 4 °C (Heraeus Megafuge 1.0R, Thermo Scientific, USA). The ferrihydrite was washed 3 times by resuspending in MilliQ water and centrifugation as described above.

All ferrihydrite minerals were stored at 4 °C in the dark. Autoclaving was omitted to avoid changes in crystal structures.

2.2 Characterization of Fe hydroxides

Fourier-transform infrared (FTIR) and Mössbauer spectroscopy measurements were performed with dialyzed (ZelluTrans, MWCO=6,000-8,000 Da, regenerated cellulose, Carl Roth, Germany) and freeze-dried (Sentry 8L, Virtis, USA) aliquots of the Fe hydroxides.

Iron speciation and magnetic properties were analyzed using a ^{57}Fe Mössbauer spectrometer (WissEl - Wissenschaftliche Elektronik GmbH, Starnberg, Germany) in transmission geometry. The measurement was performed with a ^{57}Co source in Rh matrix at room temperature, 77 K, and ~5 K. The source always remained at room temperature. A Janis closed-cycle cryostat with a helium atmosphere was used to vary the temperature of the sample. Spectra were evaluated with the Recoil software using the Voigt-based fitting method and calibrated against an α-Fe foil at room temperature. Values of the isomer or center shift are quoted relative to α-Fe at room temperature.

FTIR spectra were recorded using a Nicolet iS 10 spectrometer (Thermo Fisher Scientific, Dreieich, Germany) to study the mineral and organic composition. Mortared samples were mixed with KBr (Merck, FTIR grade) at a ratio of 1:200 and pressed to pellets. The pellets were studied in transmission mode in the mid-infrared range between 4000 and 400 cm^{-1} accumulating 16 scans per spectrum and a resolution of 4 cm^{-1}.

2.3 Humic acids preparation

Natural aquatic humic acids extracted from the deep borehole Gohy-573 in the Gorleben aquifer (Lower Saxony, Germany) were used to investigate ferrihydrite dissolution by humic acids (Buckau et al., 2000a; Buckau et al., 2000b; Wolf et al., 2004). Fractionation of humic and fulvic acids of the Gorleben groundwater was conducted by the XAD-8 method (Aiken et al., 1979; Wolf et al., 2004). The humic acid fraction was purified and characterized by elemental composition (C, H, O, N, S), inorganic constituents, proton exchange capacities, size, and mass distribution (Wolf et al., 2004) and reduction capacities were determined (Wolf et al., 2009) (see references for details).

A stock solution was prepared by adding 1 g Gohy humic acids to 1 L MilliQ water. The pH of the solution was adjusted to 7.0 with 1 M NaOH and continuously stirred over night. The humic acid solution was filtered through a 0.22 µm filter to a previously autoclaved glass bottle, sealed with a butyl rubber stopper, flushed with 20/80% CO_2/N_2, and stored at 4 °C in the dark until further use.

2.4 Microorganisms and cultivation

Geobacter sulfurreducens (Caccavo et al., 1994) DSMZ 12127 was obtained from the German Collection of Microorganisms and Cell Cultures (DSMZ, Braunschweig, Germany). The strain was cultivated using standard anaerobic techniques at 30 °C in the dark as described before (Fritzsche et al., 2012). The medium was supplemented with trace elements, selenite-tungsten, and vitamins solutions. Ten µM Na_2SO_4 was added as a sulfur source. The medium was buffered with 10 mM $NaHCO_3$ at pH 6.8. Sodium acetate was added as the sole electron source with a final concentration of 5 mM. Forty mM ferrihydrite prepared as described above was used as electron acceptor. Precultures were grown with 50 mM technical-grade ferric citrate (pH 7.0) as an electron acceptor. If not otherwise stated, all chemicals (Sigma-Aldrich, Germany) were of analytical grade.

2.5 Cell suspension

An anoxic low-salt medium was used for the batch cell suspension experiment. The cultivation medium described above was modified to 10 mg L^{-1} NaCl, 0.4 mg L^{-1} $MgCl_2 \cdot 6H_2O$, 2.5 mg L^{-1} NH_4Cl, 5 mg L^{-1} KCl, and 0.15 mg L^{-1} $CaCl_2 \cdot 2H_2O$. The medium was buffered with 10 mM Tris-HCl (pH 6.8) instead of $NaHCO_3$ to prevent the formation of minerals like e.g. siderite. All other ingredients remained unchanged.

After growth to the late exponential phase, 3 L of preculture were harvested by centrifugation for 20 min at 11,000 x g and 20 °C (Avanti J-E centrifuge with JA-10 rotor; Beckman-Coulter, USA). The cell pellet was resuspended in 50 mL fresh acetate-free low-salt medium in an anoxic glove box (O_2 < 3 ppm, N_2/H_2=95/5%, v/v, Coy Laboratory Products, USA). To remove residual citrate and acetate from the cell suspension, centrifugation and resuspension was repeated once. The cell suspension was immediately added to the reduction experiments in a 1:10 ratio and yielded final cell density of $2.2 \cdot 10^9$ cells L^{-1} in the experiment.

For normalization of reduction rates, flow cytometry was applied to measure cell numbers of the cell suspension for each individual experiment using a Cytomics FC 500 cell analyzer (Beckman-Coulter, USA). Paraformaldehyde-fixed cells from the cell suspension were stained by SYBR green I nucleic acid stain (Molecular Probes, Eugene, OR), diluted in 0.22-µm-filtered Dulbecco's phosphate-buffered saline, and counted at a wavelength of 510 nm in Trucount bead (Becton Dickson) calibrated measurements.

2.6 Microbial reduction experiments

Experiments were performed in 60-mL medium batch incubations, initiated in 100-mL glass serum bottles sealed with butyl rubber stoppers and flushed with 20/80% CO_2/N_2. Sodium acetate was added as the sole electron source with a final concentration of 5 mM. The ferrihydrite aggregates, sodium citrate solution (50 mM), and the bacterial cell suspension were added to the medium via anoxic syringes at specific amounts to obtain comparable initial ferric iron (4.2 mmol L^{-1}) and citrate (0.0 – 2.4 mM) concentrations, resulting in molar citrate/Fe ratios (citr/Fe) of 0.0 to 0.58. Ferrihydrite was incubated with medium and the respective citrate concentrations for 12 h prior to inoculation. Abiotic controls were performed by adding the cell suspension through a 0.22 µm filter (Millex-GP, Merck Millipore, USA), thereby retaining the microorganisms. Immediately after inoculation, the first samples for Fe^{2+} analysis were withdrawn. Then, the experimental bottles were incubated at 30 °C in the dark and shaken at 300 rpm.

2.7 Abiotic dissolution experiments

To study the dissolution kinetics of ferrihydrite in the presence of citrate we used the same anoxic low-salt medium as for the microbial reduction experiments (ionic strength ~10 mM,

EC ~680 µS cm^{-1}, pH 6.5). Experiments were done in triplicate 60-mL medium batch incubations, contained in 100-mL glass serum bottles sealed with butyl rubber stoppers and flushed with 20/80% CO_2/N_2. The ferrihydrite aggregates, sodium citrate solution (50 mM, pH 7.5), and Gohy humic acids (1 g L^{-1}, pH 7.0) (Wolf et al., 2009) were added to the medium via anoxic syringes to obtain comparable initial ferric iron (2.8 - 3.3 mmol L^{-1}), citrate (0.0 – 2.4 mM), and humic acid (2 – 60 mg L^{-1}) concentrations. Molar ratios of citr/Fe and organic carbon:Fe (OC/Fe) were 0.0 to 0.5 and 0.0 to 0.9, respectively. To keep the maximum volume at 90 mL, higher OC/Fe ratios were omitted. A positive control contained 4.7 mM citrate and 2.8 mM ferric iron (citr/Fe = 1.7) to ensure complete dissolution of the ferrihydrite aggregates. Immediately after addition of citrate or humic acids, the first samples for total iron content (Fe(tot)) analysis were withdrawn and centrifuged (9,700 x g, 2 min, 20 °C, Centrifuge MiniSpin®plus, Eppendorf AG, Germany). Dissolved Fe was measured as total Fe in the supernatant. Then, the experimental bottles were shaken at 300 rpm at 30 °C in the dark to avoid photo-induced reduction.

After dissolution equilibrium was reached, samples were 0.22 and 0.45 µm-filtered (Millex-GP, Merck Millipore Corp., USA) for determination of particle sizes. For mineralogical analysis, samples were centrifuged for 20 min at 4 °C with 2,900 x g (Heraeus Megafuge 1.0R, Thermo Scientific, USA) and washed three times with MilliQ water. The supernatants were dialyzed (MWCO = 6,000-8,000 Da, regenerated cellulose, Carl Roth GmbH + Co. KG, Germany) against MilliQ water until the electric conductivity of the surrounding water column remained constant (~3 µS cm^{-1}).

2.8 Determination of hydrodynamic diameters

Dynamic light scattering (DLS) was applied to measure hydrodynamic diameters (d_H) of the colloidal ferrihydrite fraction, using a ZetaSizer Nano ZS (Malvern Instruments, Worcestershire, United Kingdom) with low-volume folded capillary sizing cuvettes. Two measurements with 10 runs each were conducted per sample. The collection time per run was 10 s. Only d_H from measurements that reproducibly met the quality criteria of the software (Malvern, version 6.01) were used for interpretation. The mean polydispersity index as a measure of the size distribution of a sample with a possible maximum value of 1 for high polydispersity, was 0.242 (± 0.096; n=9) and 0.233 (± 0.051; n=9) for 0.45 µm-filtered and 0.22 µm-filtered samples, respectively.

2.9 Iron analysis

Iron was measured using the ferrozine assay (Braunschweig et al., 2012; Stookey, 1970). Aliquots of 0.2 mL were withdrawn from the experiment, diluted 1:5 in 1 M HCl, and shaken at 300 rpm for 24 h to dissolve the ferrihydrite and to remove all adsorbed Fe^{2+} from residual ferrihydrite surfaces. Total iron measurements were treated with 10% (vol/vol) hydroxylamine-HCl for a complete reduction of all Fe(III) to Fe^{2+}. Subsequently, aliquots from this aqueous ferrous iron preparation were diluted 1:10 with ferrozine, incubated for 10 min, and shaken for 30 s. Absorbance at 560 nm was measured using a Wallac 1420 Viktor^3 plate reader (Perkin Elmer, MA). Absorbance of all samples was measured in triplicates.

2.10 Quantification of citrate and humic acids

Citrate concentration was analyzed in aqueous samples using a Shimadzu LC-10A series HPLC system (Shimadzu, Japan) equipped with a Aminex HPX-87H analytical column (300 x 7.8 mm; Bio-Rad, USA) at 50 °C. Samples were analyzed by an isocratic method (5 mM H_2SO_4) at a flow rate of 0.5 mL h^{-1}. Retention time was 15.2 min and total run time was 20 min. Analytes were detected by UV absorbance at 220 nm. Samples were prepared by adding 55 µL of 35% perchloric acid to 0.5 mL of sample and incubated for 10 min on ice. Subsequently, 27 µL of 7 M KOH was added and stored at -20 °C. Before measurements, the samples were thawed at room temperature, and centrifuged at 11,330 x g for 2 minutes (Centrifuge MiniSpin®plus, Eppendorf AG, Germany).

Dissolved, non-adsorbed citrate after the experiments could not be measured, as an adsorption on ferrihydrite particles <0.45 µm could not be ruled out.

The concentration of dissolved organic carbon of the Gohy humic acid stock solution was measured with a total organic carbon analyzer TOC-5000A (Shimadzu, Kyoto, Japan) after internal acidification of the samples with 2 M HCl.

2.11 Mathematical modeling of ferrihydrite dissolution and colloid stabilization kinetics

In general the dissolution rate [mM h^{-1}] of a solid can be described by the Noyes-Whitney equation:

$$\frac{d\,C_l}{d\,t} = \frac{D \cdot A \cdot (C_s - C_l)}{L} \qquad \text{eq. (1)}$$

where *t* [h] denotes time, *D* [m^2 h^{-1}] diffusion coefficient, *A* [m^2] surface area of the solid, *L* [m] thickness of diffusion layer, and $C_s - C_l$ [mM m^{-3}] the concentration gradient between diffusion layer and bulk phase. As ferrihydrite aggregates cannot be regarded as a solid with a simple surface structure and diffusion coefficients and geometry measurements of ferrihydrite are not directly available the parameters will be summed up in the following in a single fitting parameter (named *dissolution rate constant*). The observed S-shaped nonlinear dissolution of Fe over time (Fig. 2A) revealed the multistage structure of the ferrihydrite dissolution process. The abiotic dissolution process of the large ferrihydrite aggregates (*Fh*) can be mathematically described by a spatial two-site (first-site: direct dissolution into dissolved Fe-citrate, second site: stabilization of colloids under citrate influence) and a temporal two-stage dissolution process (further dissolution of the colloidal fraction into dissolved Fe-citrate) (Fig. 6), in a system of ordinary differential equations:

$$\frac{d\ Fh}{d\ t} = -k_1 \cdot Fh - k_2 \cdot (Fh)^2 \qquad \text{eq. (2)}$$

Eq. (2) assumes that at the beginning the dissolution of *Fh* [mM] follows a first and second order reaction kinetic on two-sites, respectively, with the dissolution rate constants k_1 and k_2 [h^{-1}]. Ligand-induced dissolution of Fe hydroxides has been successfully modeled by a first-order dissolution rate process (Liang et al., 2000). Thus, we described the stabilization of ferrihydrite colloids *FeCol* [mM of total colloidal Fe] and further dissolution into dissolved Fe-citrate as it is described by eq. (3). This second-stage dissolution process depends on the difference between the initial (maximum) citrate concentration $Citr_{max}$ [mM] and the concentration of *Fh*.

$$\frac{d\ FeCol}{d\ t} = k_1 \cdot Fh - k_3 \cdot FeCol \cdot (Citr_{max} - Fh) \qquad \text{eq. (3)}$$

The dissolved Fe-citrate $FeCitr_{diss}$ [mM] is then given by the sum of first-site, second-order dissolution of *Fh* (as included in Eq.2) and second-site, second-stage dissolution of *FeCol* (including the decrease of citrate which is already bound to colloids, as included in Eq.3):

$$\frac{d\ FeCitr_{diss}}{d\ t} = k_2 \cdot (Fh)^2 + k_3 \cdot FeCol \cdot (Citr_{max} - Fh). \qquad \text{eq. (4)}$$

The ordinary differential equation system of eq. (2), (3), and (4) was numerically solved by the *NDSolve* function within the *Mathematica Software Package Version 8.0* (Wolfram Research). For testing the validity of the model, we focused on the question whether one parameter set can be used to predict the observed data arrays. Thus, one set of abiotic dissolution rate constants k_1, k_2, and k_3 was fitted for all measured dissolution curves under treatment with different citrate additions by minimizing the weighted sum of deviation squares (*SQR)* (Richter and Söndgerath, 1990) between measured and modeled dissolution. The parameter values for $Citr_{max}$ were set according to the different citrate concentrations added in the abiotic batch experiments (4.75, 1.64, 0.75, and 0.37 mM). In order to assess the adequacy of model simulations in relation to measurements, the statistically measured model efficiency (*EF*) and correlation coefficient (*r*) were used (Loague and Green, 1991). The maximum and ideal value for EF is 1.0, while a negative value indicates that model predictions are worse than using the observed mean as an estimate of the data points.

2.12 Modeling of microbial ferrihydrite reduction kinetics

Microbial reduction experiments showed that a low percentage of the ferrihydrite aggregates can be reduced by *G. sulfurreducens* without citrate addition. Microbial reduction of ferrihydrite aggregates was described by

$$\frac{d\ Fh}{d\ t} = -k_{bio,1} \cdot Fh \cdot (P_{bio,max} - Fh) \qquad \text{eq. (5)}$$

with $k_{bio,1}$ (h^{-1}) being the microbial ferrihydrite reduction rate and $P_{bio,max}$ [mM] the maximum reduction potential as given by the concentration of ferric iron. Both parameters were fitted to the measured microbial reduction rates of the control batch experiment without the addition of citrate. Eqs. (6) and (7) describe the microbial reduction of the ferrihydrite colloids and the dissolved Fe-citrate (*FeCol* and $FeCitr_{diss}$ are described in eq. 3 and 4) with the respective microbial reduction rates $k_{bio,2}$ (h^{-1}) and $k_{bio,3}$ (h^{-1}). The microbial ferrihydrite reduction can then be described by the biotic ordinary differential equation system given by eqs. (5), (6), (7), and (8).

$$\frac{d\ FeCol}{d\ t} = -k_{bio,2} \cdot FeCol \qquad \text{eq. (6)}$$

$$\frac{d\ FeCitr_{diss}}{d\ t} = -k_{bio,3} \cdot FeCitr_{diss} \quad \text{eq. (7)}$$

$$\frac{d\ FeII}{d\ t} = k_{bio,1} \cdot Fh \cdot (P_{bio,max} - Fh) + k_{bio,2} \cdot FeCol + k_{bio,3} \cdot FeCitr_{diss} \quad \text{eq. (8)}$$

Based on the relationship between citrate concentrations and abiotic dissolution and microbial reduction, microbial reduction kinetics were simulated. First, an initial ferrihydrite aggregate fraction, colloidal Fe and dissolved Fe fractions resulting from the incubation of ferrihydrite with citrate for 12 h prior to inoculation were calculated by the abiotic ordinary differential equation system and the already specified dissolution rate constants. Then, the abiotic dissolution process was continuously calculated by the abiotic ordinary differential equation system. Finally the biotic ordinary differential equation system was applied and microbial ferrihydrite aggregate reduction was continuously calculated with the already specified parameters $k_{bio,1}$ and $P_{bio,max}$, and one pair of parameters $k_{bio,2}$ and $k_{bio,3}$ was optimized for all measured reduction curves by the SQR minimization process.

The comparison of the different modelling approaches is used for the discrimination of abiotic and biotic dissolution phenomena.

3 Results

3.1 Sample characterization

Mössbauer spectroscopy of ferrihydrite incubated in citrate-free low salt medium revealed no magnetic ordering at room temperature but the onset of magnetic ordering at 77 K (Tab. 1). Magnetic ordering of citrate-incubated ferrihydrite (molar citr/Fe = 0.16) was observed at ~5 K, consistent with 2-line ferrihydrite as the single ferric Fe phase. The onset of magnetic splitting in the citrate-incubated ferrihydrite indicated a slightly higher degree of crystallinity.

The FTIR spectrum of ferrihydrite without citrate incubation showed ferrihydrite patterns with the H_2O deformation mode at 1623 cm^{-1} and symmetric and asymmetric C-O stretches at 1346 and 1463 cm^{-1}, respectively (Fig. 1). The C-O stretches probably stemmed from adsorbed carbonate of ambient CO_2 (Hausner et al., 2009). Sorption of citrate on ferrihydrite surfaces caused the formation of two broad peaks of the symmetric and asymmetric stretches of the carboxylate groups of citrate at 1382 and near 1580 cm^{-1} which

superimposed the H_2O and C-O stretches of ferrihydrite and carbonate (Fig. 1A) (Wulandari et al., 2008). With increasing citr/Fe ratio, the intensity of those two peaks also increased. A new band developed already at citr/Fe ratios of 0.04 at 1253 cm^{-1}, stemming from C-O stretches of carboxylate groups. With increasing citrate concentrations, these C-O stretches became more pronounced and a further C-O stretch at 1066 cm^{-1} occurred (Wulandari et al., 2008). Desorbed citrate caused the development of a band pair from C-H deformations at 908 and 851 cm^{-1} at a citr/Fe ratio of 0.2.

The FTIR spectrum of pure Gohy humic acids (Fig. 1B) showed aliphatic C-H stretching modes at 2928 cm^{-1} (Xiaoli et al., 2013) and symmetric stretching modes of COO^-, O-H deformation, and C-O stretching of phenolic OH at the plateau at ~1410 cm^{-1}, stemming from the aliphatic group content in the humic acids (Seddaiu et al., 2013; Xiaoli et al., 2013). Asymmetric carboxyl stretches (Wulandari et al., 2008) and C=O stretches of quinones and/or amide groups can be found at 1619 cm^{-1} (Martinez et al., 2010). The sharp peak at 1713 cm^{-1} can be assigned to C=O stretches of COOH and ketones (González Pérez et al., 2004; Martinez et al., 2010). Stretching of C-O and O-H bending of COOH groups caused the peak at 1236 cm^{-1} (Seddaiu et al., 2013). The small peaks at 1511 and 1381 cm^{-1} derived from stretch vibrations of aromatic C=C and N-H deformation vibrations (Seddaiu et al., 2013; Xiaoli et al., 2013) and symmetric COO^- stretching and/or C-O stretchings in phenols (Xiaoli et al., 2013), respectively.

Adsorption of humic acids onto ferrihydrite surfaces led to increased peak intensities of symmetric and asymmetric C-O stretches, with a shift of the symmetric deformation from 1380 cm^{-1} to 1346 cm^{-1} with decreasing C/Fe ratios (Fig. 1C).

3.2 Dissolution of ferrihydrite and colloid stabilization

Incubation of ferrihydrite with citrate resulted in partial dissolution of the ferrihydrite within the first 70 h when citrate concentrations were > 0.5 mM (Fig. 2A). With increasing molar citr/Fe ratios, the amount of released Fe increased up to 93% at a ratio of 0.5 and reached 100% at a ratio of 1.7 of the positive control. Dissolution rates increased from 6.4 µM h^{-1} (citr/Fe = 0.1) up to 37 µM h^{-1} (citr/Fe = 1.7) (Fig. 2A). The pH remained at a constant level of approximately 6.3 over the entire experiment.

Incubation of ferrihydrite with humic acids did not lead to a detectable dissolution of ferrihydrite after 71 d (Fig. 2B). The pH decreased slightly from 6.1 ± 0.1 to 5.5 0.1 during the experiment.

After filtration of the samples, both the positive control (citr/Fe = 1.7) and the citr/Fe = 0.5 sample showed a 100% recovery of the total initial Fe concentration (Fig. 2C). Iron concentrations in the filtrates of samples with molar citr/Fe ratios between 0.1 and 0.5 were at least twice as high as the citrate concentrations. No citrate or Fe was detectable in filtrates of samples without citrate or with a citr/Fe ratio of 0.01. No Fe was detected in filtrates of ferrihydrite incubated with humic acids (data not shown).

In samples with citr/Fe ratios between 0.1 and 0.5, colloidal dispersed particles with declining hydrodynamic diameters between 89 (± 53) – 165 (± 65) nm and 69 (± 37) – 115 (± 52) nm were detected in 0.45 and 0.22 µm-filtrates, respectively. Zeta potentials of these particles were between -38.4 (± 0.5) mV and -41.2 (± 1.1) mV. In our experimental setup no particles could be detected in humic acids-containing samples (data not shown).

3.3 Microbial reduction by G. sulfurreducens

Microbial reduction of ferrihydrite incubated with different citrate concentrations revealed increasing initial reduction rates with increasing citrate concentrations, except for a citr/Fe ratio of 0.03 (Fig. 3). Here, the reduction rates decreased slightly from 28.6 ± 2.7 µM h^{-1} (without citrate) to 22.9 ± 0.8 µM h^{-1}. Complete reduction was reached after 30 h for a citr/Fe ratio of 0.58 and after 74 h for ratios of 0.14 and 0.27 (Fig. 3).

3.4 Modeling results of abiotic ferrihydrite dissolution and colloid stabilization kinetics

For the quantitative description of the citrate-induced dissolution of ferrihydrite the system of ordinary differential equations Eq. (2), (3), and (4) was solved numerically. The minimization of the *SQR* value for the modeling results of $FeCitr_{diss}$ with respect to measurements resulted in a set of dissolution rate constants (Tab. 2).

Figure 4 shows the simulated abiotic ferrihydrite dissolution kinetics with a simultaneous stabilization of ferrihydrite colloids, and mean values of measured dissolved Fe citrate after different citrate additions. As the observed dissolution rates of ferrihydrite in the first 10 hours were nearly in the same range for the different treatments, it was assumed in the

ordinary differential equation system that the added citrate amounts mainly influenced the dissolution of the initially present colloidal ferrihydrite fraction to Fe citrate.

The low overall *SQR* value of 1.227 and the high values for the modeling efficiency and the correlation coefficient close to the maximum value 1.0 showed that the optimization results are of good quality (Tab. 3) and that one parameter set of abiotic dissolution rate constants can be used to predict the observed data arrays of dissolved Fe fractions. The negative EF value for the citr/Fe ratio of 0.1 indicates that model predictions are worse compared to measured values, but as the *r* value is also high it can be assumed that the simulation results are valid.

3.5 Modeling results of microbial reduction kinetics

For the quantitative description of the microbial ferrihydrite reduction after citrate addition, the abiotic and biotic ordinary differential equation systems were numerically solved. For the control batch experiment, a value of the maximum reduction potential $P_{bio,max}$ = 4.4 mM was estimated by the SQR minimization procedure. The minimization of the *SQR* value for the modeling results of microbial Fe reduction (*FeII*) resulted in a microbial aggregate reduction rate and one set of biotic reduction rate constants (Tab. 4). As expected, the parameter optimization resulted in a 2.5-fold higher microbial reduction rate for the dissolved Fe citrate fraction (0.1 h^{-1}) rather than for the colloidal fraction (0.04 h^{-1}), yet the colloidal fraction also showed a much higher bioavailability than the ferrihydrite aggregates (0.04 h^{-1} > 0.011 h^{-1}).

Figure 5 shows the simulated microbial ferrihydrite reduction kinetics for different citrate additions, the control (citr/Fe = 0.0), and mean values of measured reduced Fe. Good optimization results were obtained for the control and for a citr/Fe ratio of 0.27, indicated by the low overall *SQR* value of 2.263 and the high *EF* and *r* values close to the maximum value 1.0 (Tab. 3). The differences in microbial Fe reduction between the different citrate treatments after 8 h were underestimated by the modeling results compared to the measurements. This was reflected in the lower modeling efficiency values for the treatments with citr/Fe ratios of 0.14 and 0.58.

4 Discussion

4.1 Sample characterization

Moessbauer spectroscopy showed that both ferrihydrite incubated in citrate-free microbial low salt medium and ferrihydrite incubated with citrate were pure 2-line ferrihydrites (Kukkadapu et al., 2003). The onset of magnetic ordering at 77 K of citrate-free ferrihydrite revealed a slightly higher crystallinity compared to ferrihydrite incubated with citrate. Different publications (Barrón and Torrent, 2002; Barrón et al., 2003; Michel et al., 2010) described the transformation of synthetic 2-line ferrihydrite to a mixture of 6-line ferrihydrite, hematite, and hydromaghemite in the presence of citrate at elevated temperatures of at least 100 °C. An increase of magnetic susceptibility was observed for ferrihydrite-citrate coprecipitates at moderate temperatures of 25 and 50 °C (Cabello et al., 2009). Those recrystallization processes can be excluded for ferrihydrite samples with adsorbed citrate in the present study because no evidence for increased magnetic splitting was found (Tab. 1). Beginning transformation to higher crystalline Fe hydroxides of pure ferrihydrite at incubation temperatures of 30 °C might have caused the slightly higher crystallinity compared to ferrihydrite-citrate incubations, although no other Fe hydroxides were detected. Most likely recrystallization of citrate-incubated ferrihydrite (citr/Fe = 0.16) was inhibited due to little aggregation caused by adsorbed citrate (Cornell, 1987).

Adsorption of citrate onto ferrihydrite surfaces led to an intense increase of symmetric and asymmetric C-O stretching modes (Fig. 1A). Three COO^- groups of citrate are responsible for its anchoring on surfaces resulting in peak maxima near 1590 cm^{-1} for asymmetric stretching and at 1380 and 1440 cm^{-1} for symmetric stretching deformations (Wulandari et al., 2008). Dialysis of ferrihydrite-citrate samples resulted in a single symmetric stretching peak at 1380 cm^{-1} (Wulandari et al., 2008), probably due to formation of inner-sphere complexes (Mudunkotuwa and Grassian, 2010). The symmetric C-O stretch at 1346 cm^{-1} shifted also to higher wavenumbers for adsorbed humic acids at OC/Fe ratios of 0.3 and 0.9, suggesting a similar inner-sphere complexation as for Fe-citrate. Furthermore, the asymmetric C-O stretching mode shifts to lower frequencies at an OC/Fe ratio of 0.9, caused by weaker outer-sphere complexes (Eusterhues et al., 2011).

4.2 Ferrihydrite dissolution and colloid stabilization

Abiotic citrate-induced dissolution rates of ferrihydrite increased with increasing initial citrate concentrations (Fig. 2A) which is in accordance with Liang et al. (Liang et al., 2000). Since ferrihydrite is an aggregated Fe hydroxide consisting of crystallites in the size range between 2 to 6 nm (Vodyanitskii, 2010) the surface site density for citrate adsorption is higher compared to other Fe hydroxides. Citrate adsorption onto these "inner surfaces" between aggregated particles leads to repulsive forces between these particles and therefore to disaggregation. According to the DLVO theory (Derjaguin and Landau, 1941; Verwey and Overbeek, 1948) attractive forces dominate if the electrochemical double layer shrinks due to neutralization of the positive surface charge of pure ferrihydrite after adsorption of a few citrate anions. This effect can be seen at a citr/Fe ratio of 0.01 (Fig. 2A). Here, no ferrihydrite disaggregation was detected. At increasing citrate concentrations, the surface charge of ferrihydrite turned to negative values, resulting in electrostatic repulsion forces between single particles and formation of a stable colloidal suspension from large ferrihydrite aggregates. Similar observations were described in a study on ferrihydrite coated quartz sand columns (Liang et al., 2000). The citrate-containing influent led to the release of ferrihydrite colloids from the ferrihydrite surface coating. The authors suggested that electrostatic forces between citrate coated quartz sand and citrate coated ferrihydrite led to repulsion between these different compounds. However, we suggest that citrate coatings may cause also electrostatic repulsive forces between small aggregated moieties within large ferrihydrite aggregates. In our experiments, these electrostatic repulsion forces probably resulted in the disintegration of ferrihydrite aggregates to colloids of about 70 – 165 nm in hydrodynamic diameter at citr/Fe ratios of at least 0.1 (Fig. 2C). Our simulation results showed that after low (citr/Fe ratios ~0.1) and high citrate (citr/Fe ratios ~1.7) additions comparable colloid stabilization processes occurred (Fig. 4). Further dissolution into dissolved Fe citrate fractions is accelerated at high citrate availability. The simulation results thus confirmed that even low citrate concentrations can cause electrostatic repulsive forces between small individual ferrihydrite aggregates, and that colloid stabilization was initiated accordingly. Both particles and turbidity were not detectable at a citr/Fe ratio > 1, because of a complete dissolution of ferrihydrite with excess citrate (Fig. 2C).

Formation of a stable colloidal suspension also explained the higher Fe concentrations relative to citrate in filtrates of samples with citr/Fe ratios of 0.1 – 0.5. According to Martin (Martin, 1986), $FeCitrH_{-1}^{-}$ complexes dominate over $FeCitr_2^{3-}$ at pH values between 6 and 7.

Consequently, we expected citr/Fe ratios of about 1 in filtrates if dissolution is the only ferrihydrite disintegrating process taking place. However, our results showed an actual ratio of ~0.4, which can be well explained by the presence of citrate-coated ferrihydrite colloids.

The nonlinear dissolution of ferrihydrite over time (Fig. 2A) can be attributed to the polydisperse nature of ferrihydrite, with aggregates and smaller particles present as it was proposed by Liang et al. (Liang et al., 2000). Smaller particles dissolve faster than aggregated ferrihydrite resulting in a decrease of initial dissolution after disappearance of small particles. In our experiments, the decreasing dissolution rate within the first 10 h could be described by the ordinary differential equation system of eq. 2, 3, and 4 under the assumption that the amount of added citrate mainly influenced the dissolution of initially present colloids.

After citrate adsorption to the ferrihydrite aggregate surfaces, ligand exchange reactions between ferrihydrite and citrate started. These dissolution reactions weaken the intra-aggregate structure. Together with electrostatic repulsion forces between smaller aggregates, this leads to separation and formation of a stable colloidal suspension/dispersion.

At a citr/Fe ratio of 0.1 approximately all citrate molecules were mainly adsorbed onto the surfaces of the initially present colloidal fraction and led to ferrihydrite dissolution by ligand exchange. Further dissolution was not possible since all citrate was bound to ferric Fe. Probably, with further addition of citrate, negatively charged ferric citrate adsorbed onto surfaces of sub-aggregates, leading to further colloid stabilization by electrostatic repulsion forces, causing similarly high colloid concentrations for citr/Fe ratios between 0.1 and 0.5.

At citr/Fe ratios > 0.1 a certain amount of Na_3-citrate remained in solution at the time point where a certain amount of ferrihydrite was disaggregated and formed a stable colloidal suspension. Caused by this colloid stabilization the available surface area and the amount of sorption sites for citrate increased leading to an accelerated dissolution after ~10 h compared to citr/Fe = 0.1 (Fig. 4). With increasing citr/Fe ratios the influence of the dissolution of the colloids increased, leading to lower colloid concentrations (Fig. 4).

Based on these results we propose the following ferrihydrite-dissolution mechanism (Fig. 6):

(i) adsorption of citrate on initially present ferrihydrite colloid surfaces

(ii) fast dissolution of small, less aggregated particles

(iii) adsorption of citrate onto surfaces of ferrihydrite aggregates until saturation of sorption sites occurs

(iv) weakening of the surface structure induced by ligand exchange

(v) electrostatic stabilization of smaller, aggregated particles due to citrate coating and stabilization of colloids, resulting in an increased amount of available surface sorption sites

(vi) fast adsorption of residual citrate onto new colloidal surfaces and dissolution according to the model of Furrer and Stumm (Furrer and Stumm, 1986).

The used Gohy humic acids did not lead to a detectable stabilization of colloids from ferrihydrite aggregates in our experiments. In contrast to citrate, humic acids dissolved less Fe from ferrihydrite (Fig. 2B) leading to less disaggregation of the aggregate surfaces compared to citrate.

4.3 Microbial reduction of ferrihydrite in the presence of citrate

Initial microbial reduction rates of ferrihydrite incubated with *G. sulfurreducens* increased with increasing citrate concentrations exceeding a critical minimum concentration (Fig. 3). No enhanced reduction was observed at a citr/Fe ratio of 0.03 compared to a ratio of 0.0. This observation was probably caused by the strengthening of aggregates due to surface charge neutralization and therefore decreased bioaccessibility of Fe. Differences of initial reduction rates of samples with citr/Fe ratios between 0.14 and 0.58 are rather low (0.146 – 0.184 mM h^{-1}) suggesting that maximum reduction rates are almost reached at a citr/Fe ratio of 0.14.

The modeling of the coupled mechanism of citrate-induced dissolution and colloid stabilization from ferrihydrite aggregates with microbial reduction processes could reproduce the observed Fe reduction capability of the batch system (Fig. 5). The underestimation in the reduction kinetic simulation for the citr/Fe ratio of 0.58 can be explained by the fact that the stably dispersed colloidal fractions after 12 h incubation (prior to inoculation with *G. sulfurreducens*) are relatively high with ~2.0 – 2.6 mM (Fig. 4). Furthermore, the differences between calculated initially dissolved fractions ($FeCitr_{diss}$ = 0.19 mM for citr/Fe ratio 0.14 compared to $FeCitr_{diss}$ = 0.47 mM for citr/Fe ratio 0.58) are rather small. Although dissolution and colloid stabilization processes were continuously calculated in the present simulation, individual differences caused by respective citr/Fe ratios could not

be described with a single parameter set as it was used for the calculations in our study. Therefore, the model underestimates the microbial reduction rate at a citr/Fe ratio of 0.58. However, the simulation results indicate that also the colloidal Fe fraction is highly bioavailable in the system and can be reduced by *G. sulfurreducens* with a rate of 0.04 h^{-1}. Our results indicated that the influence of stably dispersed colloids is more pronounced at low citrate concentrations because the dissolved Fe citrate fraction is rather small.

The coupled mechanism of citrate-induced dissolution and colloid stabilization from ferrihydrite aggregates also explains the catalytic effect of citrate-bearing colloidal ferrihydrite on ferrihydrite aggregate reduction in a recent study (Bosch et al., 2010). Similar to the present study, cell suspension experiments with *G. sulfurreducens*, grown on ferric citrate were conducted. In contrast to our study, the cell pellets were washed only once instead of twice, leading to citrate concentrations of ~1 mM in the cell suspensions which were added to the ferrihydrite phase. In combination with 10% citrate-containing colloids this led to a final citrate concentration of ~0.1 mM. According to the results presented here, this should have resulted in the stabilization of additional colloids from larger aggregates, strongly increasing the reduction rates. Regarding our results, this cannot be ascribed to a catalytic effect of ferrihydrite colloids on microbial ferrihydrite reduction but to an increased amount of suspended colloids. In experiments with only ferrihydrite aggregates and without citrate-containing colloids, the added citrate from the cell suspension had no effect because the concentration was too low, probably with a molar citr/Fe ratio «0.1. This led to stronger aggregation of ferrihydrite particles and therefore no enhancement of microbial reduction. In the light of this finding, we exclude the formerly proposed function of ferrihydrite colloids as electron shuttles (Bosch et al., 2010).

Gohy humic acids did not induce colloid stabilization in our experiments. Enhancement of microbial Fe hydroxide reduction in the presence of Gohy humic acids can therefore be attributed to electron shuttling between microbial cells and Fe hydroxides (Wolf et al., 2009). However, Fe hydroxides produced by coprecipitation of humics with ferric iron might exhibit other properties (Pédrot et al., 2011).

5 Conclusions and environmental implications

Until now, the impact of low molecular weight organic acids like citrate was thought to be restricted to increasing the solubility of minerals, to improve the uptake of Fe or phosphorous by plant roots, and to enhance microbial mineral accessibility. Our results prove that also the additional electrostatic stabilization of colloids at molar citr/Fe ratios of environmental significance increases microbial Fe hydroxide reduction significantly. At low citr/Fe ratios, colloid stabilization might be distinctively more important than dissolution of ferrihydrite. Especially in soils where low molecular weight organic acids are excreted by plant roots, organics-mediated colloid stabilization might play an important role as source of mobile Fe colloids and therefore for microbial bioavailability of Fe hydroxides. The reactivity of Fe hydroxides increases with disintegration of larger particles or aggregates to smaller colloids which might lead to increased microbial turnover rates of Fe hydroxides in the environment.

In groundwater, the concentrations of low molecular weight organic acids are negligible. Here, refractory organic substances like humic or fulvic acids dominate. Since these substances did not lead to similar colloid stabilization as low molecular weight organic acids in our experiments, we propose that mainly their function as electron shuttle is causing higher microbial reduction rates of Fe hydroxides. Therefore, it is likely that electron shuttling compounds play a dominant role in Fe hydroxide reduction in aquifers. Their importance probably decreases in soils and sediments with increasing concentrations of low molecular weight organic acids, leading to dissolution and stabilization of highly bioavailable Fe hydroxide colloids. However, the situation might be different for natural Fe hydroxides formed in the environment because they contain internally bound natural organic molecules incorporated during precipitation.

Acknowledgments

We thank Sviatlana Marozava for HPLC measurements. This study was funded by the research group FOR 580 of the German Research Foundation (DFG) “Electron Transfer Processes in Anoxic Aquifers”, the Nanosan project of the German Federal Ministry of Education (BMBF, Grant ID 03X0085A), and the EU-project NANOREM (FP7-Grant Agreement #309517). We gratefully acknowledge the European Science Foundation (ESF) and its Research Networking Programme 'The Functionality of Iron Minerals in Environmental Processes'.

References

Aiken, G.R., Thurman, E.M., Malcolm, R.L. and Walton, H.F. (1979) Comparison of XAD macroporous resins for the concentration of fulvic acid from aqueous solution. Anal. Chem. 51, 1799-1803.

Allard, T., Weber, T., Bellot, C., Damblans, C., Bardy, M., Bueno, G., Nascimento, N.R., Fritsch, E. and Benedetti, M.F. (2011) Tracing source and evolution of suspended particles in the Rio Negro Basin (Brazil) using chemical species of iron. Chem. Geol. 280, 79-88.

Amstaetter, K., Borch, T. and Kappler, A. (2012) Influence of humic acid imposed changes of ferrihydrite aggregation on microbial Fe(III) reduction. Geochimica Et Cosmochimica Acta 85, 326-341.

Anderson, H.A., Berrow, M.L., Farmer, V.C., Hepburn, A., Russell, J.D. and Walker, A.D. (1982) A reassessment of podzol formation processes. J. Soil Sci. 33, 125-136.

Barrón, V. and Torrent, J. (2002) Evidence for a simple pathway to maghemite in Earth and Mars soils. Geochim. Cosmochim. Acta 66, 2801-2806.

Barrón, V., Torrent, J. and de Grave, E. (2003) Hydromaghemite, an intermediate in the hydrothermal transformation of 2-line ferrihydrite into hematite. Am. Mineral. 88, 1679-1688.

Bosch, J., Heister, K., Hofmann, T. and Meckenstock, R.U. (2010) Nanosized iron oxide colloids strongly enhance microbial iron reduction. Appl. Environ. Microbiol. 76, 184-189.

Braunschweig, J., Bosch, J., Heister, K., Kuebeck, C. and Meckenstock, R.U. (2012) Reevaluation of colorimetric iron determination methods commonly used in geomicrobiology. J. Microbiol. Methods 89, 41-48.

Buckau, G., Artinger, R., Fritz, P., Geyer, S., Kim, J.I. and Wolf, M. (2000a) Origin and mobility of humic colloids in the Gorleben aquifer system. Appl. Geochem. 15, 171-179.

Buckau, G., Artinger, R., Geyer, S., Wolf, M., Fritz, P. and Kim, J.I. (2000b) Groundwater in-situ generation of aquatic humic and fulvic acids and the mineralization of sedimentary organic carbon. Appl. Geochem. 15, 819-832.

Buurman, P. and Jongmans, A.G. (2005) Podzolisation and soil organic matter dynamics. Geoderma 125, 71-83.

Cabello, E., Morales, M.P., Serna, C.J., Barrón, V. and Torrent, J. (2009) Magnetic enhancement during the crystallization of ferrihydrite at 25 and 50 °C. Clay. Clay Min. 57, 46-53.

Caccavo, F., Lonergan, D.J., Lovley, D.R., Davis, M., Stolz, J.F. and McInerney, M.J. (1994) *Geobacter sulfurreducens* sp. nov., a hydrogen- and acetate oxidizing dissimilatory metal-reducing microorganism. Appl. Environ. Microbiol. 60, 3752-3759.

Cornell, R.M. (1987) Comparison and classification of the effects of simple ions and molecules upon the transformation of ferrihydrite into more crystalline products. Z. Pflanzenernähr. Bodenk. 150, 304-307.

de Corninck, F. (1980) Major mechanisms in formation of spodic horizons. Geoderma 24, 101-128.

Derjaguin, B. and Landau, L. (1941) Theory of the stability of strongly charged lyophobic sols and of the adhesion of strongly charged particles in solutions of electrolytes. Acta Physico Chemica 14, 633.

do Nascimento, N.R., Bueno, G.T., Fritsch, E., Herbillon, A.J., Allard, T., Melfi, A.J., Astolfo, R., Boucher, H. and Li, Y. (2004) Podzolization as a deferralitization process: a study of an Acrisol-Podzol sequence derived from Palaeozoic sandstones in the northern upper Amazon Basin. Eur. J. Soil Sci. 55, 523-538.

Eusterhues, K., Rennert, T., Knicker, H., Koegel-Knabner, I., Totsche, K.U. and Schwertmann, U. (2011) Fractionation of organic matter due to reaction with ferrihydrite: coprecipitation versus adsorption. Environ. Sci. Technol. 45, 527-533.

Fritzsche, A., Bosch, J., Rennert, T., Heister, K., Braunschweig, J., Meckenstock, R.U. and Totsche, K.U. (2012) Fast microbial reduction of ferrihydrite colloids from a soil effluent. Geochim. Cosmochim. Acta 77, 444-456.

Furrer, G. and Stumm, W. (1986) The coordination chemistry of weathering: I. Dissolution kinetics of αAl_2O_3 and BeO. Geochim. Cosmochim. Acta 50, 1847-1860.

González Pérez, M., Martin-Neto, L., Saab, S.C., Novotny, E.H., Milory, D.M.B.P., Bagnato, V.S., Colnago, L.A., Melo, W.J. and Knicker, H. (2004) Characterization of humic acids from a Brazilian Oxisol under different tillage systems by EPR, ^{13}C NMR, FTIR and fluorescence spectroscopy. Geoderma 118, 181-190.

Hashimoto, Y. (2007) Citrate sorption and biodegradation in acid soils with implications for aluminum rhizotoxicity. Appl. Geochem. 22, 2861-2871.

Hausner, D.B., Bhandari, N., Pierre-Louis, A.-M., Kubicki, J.D. and Strongin, D.R. (2009) Ferrihydrite reactivity toward carbon dioxide. J. Colloid Interface Sci. 337, 492-500.

Hochella, M.F., Lower, S.K., Maurice, P.A., Penn, R.L., Sahai, N., Sparks, D.L. and Twining, B.S. (2008) Nanominerals, mineral nanoparticles, and Earth systems. Science 319, 1631-1635.

IUPAC (1997) Compendium of chemical terminology, 2nd edn, compiled by McNaught, A. D., Wilkinson, A., in: McNaught, A.D., Wilkinson, A. (Eds.), 2 ed. Blackwell Scientific Publications, Oxford.

Jones, D.L. and Brassington, D.S. (1998) Sorption of organic acids in acid soils and its implications in the rhizosphere. Eur. J. Soil Sci. 49, 447-455.

Kraemer, S.M. and Hering, J.G. (1997) Influence of solution saturation state on the kinetics of ligand-controlled dissolution of oxide phases. Geochim. Cosmochim. Acta 61, 2855-2866.

Kukkadapu, R.K., Zachara, J.M., Fredrickson, J.K., Smith, S.C., Dohnalkova, A.C. and Russell, C.K. (2003) Transformation of 2-line ferrihydrite to 6-line ferrihydrite under oxic and anoxic conditions. Am. Miner. 88, 1903-1914.

Lackovic, K., Johnson, B.B., Angove, M.J. and Wells, J.D. (2003) Modeling the adsorption of citric acid onto Muloorina illite and related clay minerals. J. Colloid Interface Sci. 267, 49-59.

Liang, L., Hofmann, A. and Gu, B. (2000) Ligand-induced dissolution and release of ferrihydrite colloids. Geochim. Cosmochim. Acta 64, 2027-2037.

Loague, K. and Green, R.E. (1991) Statistical and graphical methods for evaluating solute transport models: overview and application. J. Contaminant Hydrol. 7, 51-73.

Lovley, D.R. and Phillips, E.J.P. (1986) Organic matter mineralization with reduction of ferric iron in anaerobic sediments. Appl. Environ. Microbiol. 51, 683-689.

Lundström, U.S. (1994) Significance of organic acids for weathering and the podzolization process. Environ. Int. 20, 21-30.

Lundström, U.S., van Breemen, N. and Bain, D. (2000) The podzolization process. A review. Geoderma 94, 91-107.

Madden, A.S. and Hochella, M.F. (2005) A test of geochemical reactivity as a function of mineral size: manganese oxidation promoted by hematite nanoparticles. Geochim. Cosmochim. Acta 69, 389-398.

Madden, A.S., Hochella, M.F. and Luxton, T.P. (2006) Insights for size-dependent reactivity of hematite nanomineral surfaces through Cu^{2+} sorption. Geochim. Cosmochim. Acta 70, 4095-4104.

Martin, R.B. (1986) Citrate binding of Al^{3+} and Fe^{3+}. J. Inorg. Biochem. 28, 181-187.

Martinez, R.E., Sharma, P. and Kappler, A. (2010) Surface binding site analysis of Ca^{2+}-homoionized clay-humic acid complexes. J. Colloid Interface Sci. 352, 526-534.

Michel, F.M., Barrón, V., Torrent, J., Morales, M.P., Serna, C.J., Boily, J.-F., Liu, Q., Ambrosini, A., Cismasu, A.C. and Brown Jr, G.E. (2010) Ordered ferrimagnetic form of ferrihydrite reveals links among structure, composition and magnetism. PNAS 107, 2787-2792.

Mikutta, C., Frommer, J., Voegelin, A., Kaegi, R. and Kretzschmar, R. (2010) Effect of citrate on the local Fe coordination in ferrihydrite, arsenate binding, and ternary arsenate complex formation. Geochim. Cosmochim. Acta 74, 5574-5592.

Miller, W.P., Zelazny, L.W. and Martens, D.C. (1986) Dissolution of synthetic crystalline and noncrystalline iron oxides by organic acids. Geoderma 37, 1-13.

Mudunkotuwa, I.A. and Grassian, V.H. (2010) Citric acid adsorption on TiO_2 nanoparticles in aqueous suspensions at acidic and circumneutral pH: surface coverage, surface speciation, and its impact on nanoparticle-nanoparticle interaction. J. Am. Chem. Soc. 132, 14986-14994.

Oburger, E., Leitner, D., Jones, D.L., Zygalakis, K.C., Schnepf, A. and Roose, T. (2011) Adsorption and desorption dynamics of citric acid anions in soil. Eur. J. Soil Sci. 62, 733-742.

Pédrot, M., Le Boudec, A., Davranche, M., Dia, A. and Henin, O. (2011) How does organic matter constrain the nature, size and availability of Fe nanoparticles for biological reduction. J. Colloid Interface Sci. 359, 75-85.

Piepenbrock, A., Schroder, C. and Kappler, A. (2014) Electron Transfer from Humic Substances to Biogenic and Abiogenic Fe(III) Oxyhydroxide Minerals. Environmental Science & Technology 48, 1656-1664.

Richter, O. and Söndgerath, D. (1990) Parameter estimation in ecology. VCH Publishers, Weinheim.

Riise, G., van Hees, P., Lundström, U. and Strand, L.T. (2000) Mobility of different size fractions of organic carbon, Al, Fe, Mn and Si in podzols. Geoderma 94, 237-247.

Roden, E.E. (2003) Fe(III) oxide reactivity toward biological versus chemical reduction. Environ. Sci. Technol. 37, 1319-1324.

Roden, E.E. (2012) Microbial iron-redox cycling in subsurface environments. Biochem. Soc. T. 40, 1249-1256.

Seddaiu, G., Porcu, G., Ledda, L., Roggero, P.P., Agnelli, A. and Corti, G. (2013) Soil organic matter content and composition as influenced by soil management in a semi-arid Mediterranean agro-silvo-pastoral system. Agr. Ecosyst. Environ. 167, 1-11.

Stookey, L.L. (1970) Ferrozine: a new spectrophotometric reagent for iron. Anal. Chem. 42.

Stumm, W. and Furrer, G. (1987) The dissolution of oxides and aluminum silicates; examples of surface coordination-controlled kinetics, in: Stumm, W. (Ed.), Aquatic surface chemistry. Chemical processes at the particle-water interface. Wiley, New York.

van Hees, P.A.W. and Lundström, U.S. (2000) Equilibrium models of aluminium and iron complexation with different organic acids in soil solution. Geoderma 94, 201-221.

van Hees, P.A.W., Lundström, U.S. and Giesler, R. (2000) Low molecular weight organic acids and their Al-complexes in soil sulution - composition, distribution and seasonal variation in three podzol soils. Geoderma 94, 173-200.

Verwey, E.J.W. and Overbeek, J.T.G. (1948) Theory of the stability of lyophobic colloids. Elsevier.

Vodyanitskii, Y.N. (2010) Iron hydroxides in soils: a review of publications. Eurasian Soil. Sci. 43, 1244-1254.

Waychunas, G.A., Kim, C.S. and Banfield, J.F. (2005) Nanoparticulate iron oxide minerals in soils and sediments: unique properties and contaminant scavenging mechanisms. J. Nanopart. Res. 7, 409-433.

Weber, K.A., Achenbach, L.A. and Coates, J.D. (2006) Microorganisms pumping iron: anaerobic microbial iron oxidation and reduction. Nat. Rev. Micro. 4, 752-764.

Wolf, M., Buckau, G. and Geyer, S. (2004) Isolation and characterization of new batches of Gohy-573 humic and fulvic acids, in: Buckau, G. (Ed.), In *Humic substances in performance assessment of nuclear waste disposal: actinide and iodine migration in the far-field*. Forschungszentrum Karlsruhe, Karlsruhe, pp. 111-124.

Wolf, M., Kappler, A., Jiang, J. and Meckenstock, R. (2009) Effects of humic substances and quinones at low concentrations on ferrihydrite reduction by *Geobacter metallireducens*. Environ. Sci. Technol. 43, 5679-5685.

Wulandari, P., Li, X.H., Tamada, K. and Hara, M. (2008) Conformational study of citrates adsorbed on gold nanoparticles using Fourier transform infrared spectroscopy. J. Nonlinear Opt. Phys. 17, 185-192.

Xiaoli, C., Yongxia, H., Guixiang, L., Xin, Z. and Youcai, Z. (2013) Spectroscopic studies of the effect of aerobic conditions on the chemical characteristics of humic acid in landfill leachate and its implication for the environment. Chemosphere 91, 1058-1063.

Yan, B., Wrenn, B.A., Basak, S., Biswas, P. and Giammar, D.E. (2008) Microbial reduction of Fe(III) in hematite nanoparticles by *Geobacter sulfurreducens*. Environ. Sci. Technol. 42, 6526-6531.

Figures

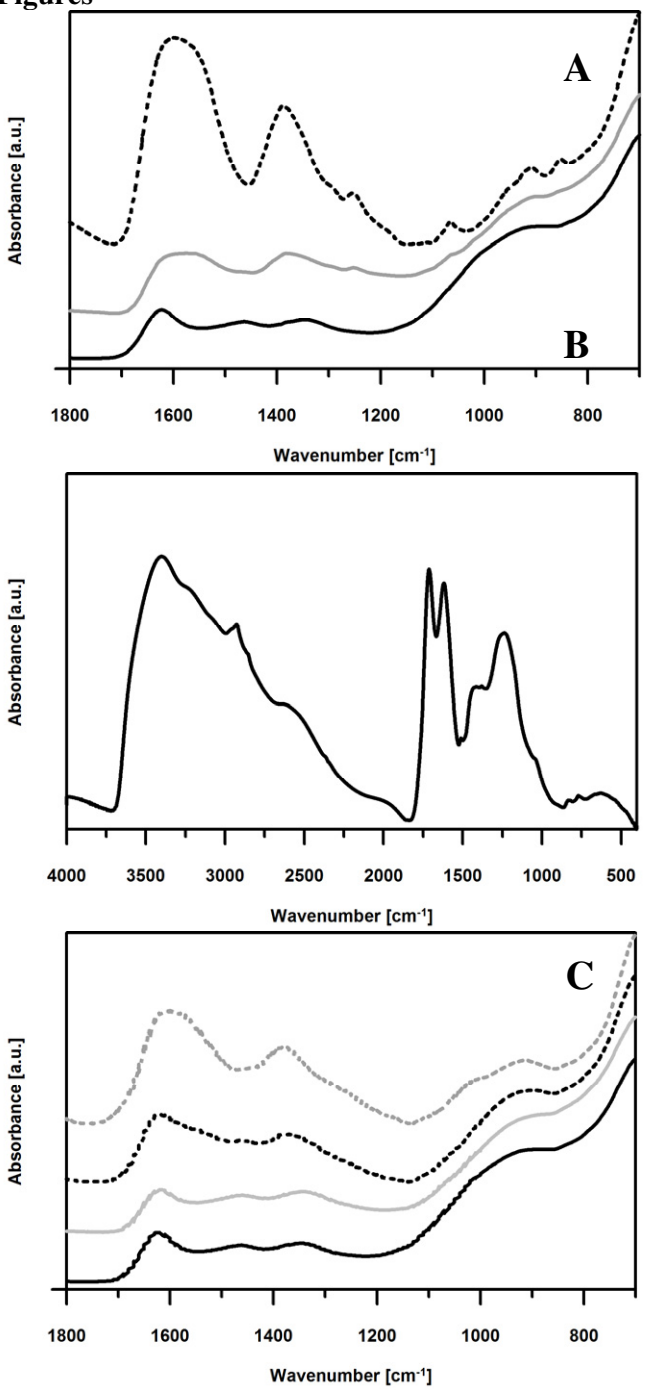

Fig. 1: FTIR spectra of ferrihydrite incubated with different citrate concentrations (A) with molar citr:Fe ratios of 0.0 (solid black line), 0.04 (solid grey line), and 0.2 (dotted black line), of pure Gohy humic acids (B) and humic acids associated with ferrihydrite (C) with molar organic carbon (OC):Fe ratios of 0.0 (solid black line), 0.03 (solid grey line), 0.3 (dotted black line), and 0.9 (dotted grey line). Absorbance is given in arbitrary units (a.u.).

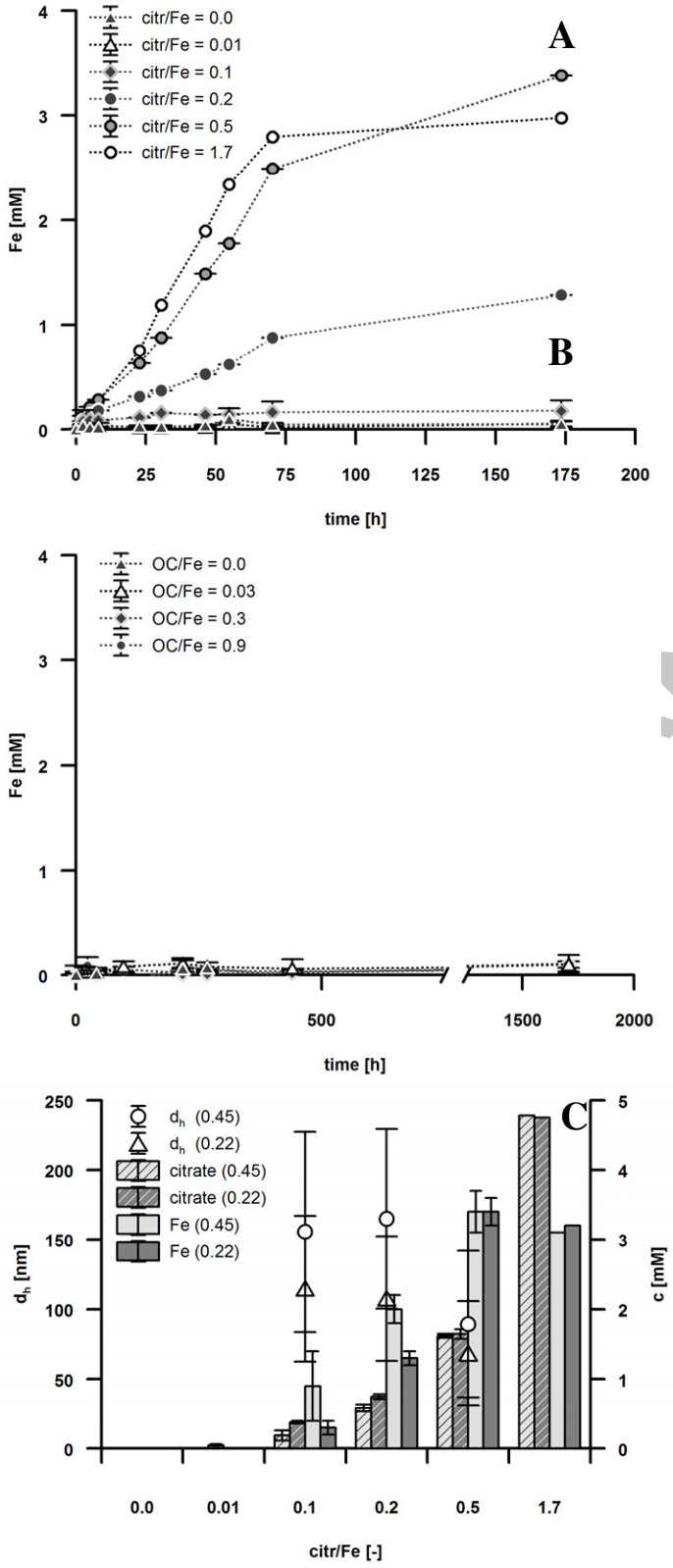

Fig. 2: Abiotic dissolution of ferrihydrite with citrate (A) at molar citr:Fe ratios of 0.0-1.7 (average total Fe concentration: 3.3 (± 0.3) mM) and humic acids (B) at molar organic carbon (OC):Fe ratios of 0.0-0.9 (average total Fe concentration: 2.9 (± 0.3) mM). Grey and striped bars depict Fe concentrations [mM total Fe] and citrate concentrations in filtrates,

respectively; dots and triangles show hydrodynamic diameters (d_h) of detected colloids (C). Error bars depict standard deviations of three measurements of three replicate experiments.

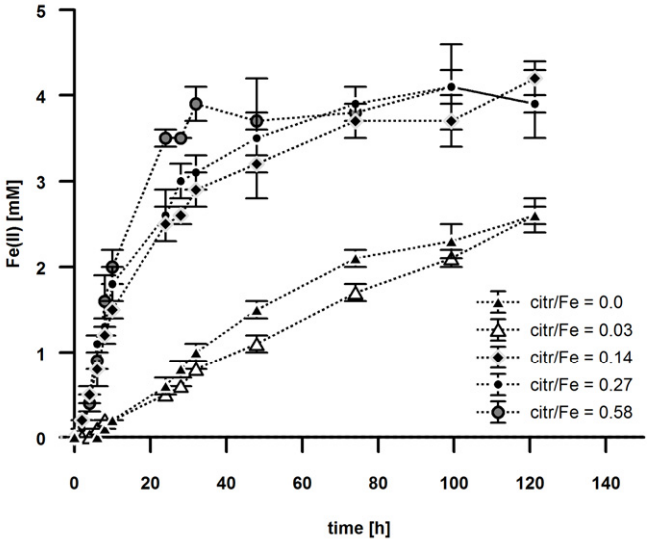

Fig. 3: Microbial reduction of ferrihydrite by *Geobacter sulfurreducens* incubated at different citrate concentrations with molar citr:Fe ratios of 0.0-0.58. Average total Fe concentrations of all samples: 3.9 ± 0.1 mM (n=15). Error bars depict standard deviations of triplicate measurements of three biological replicates.

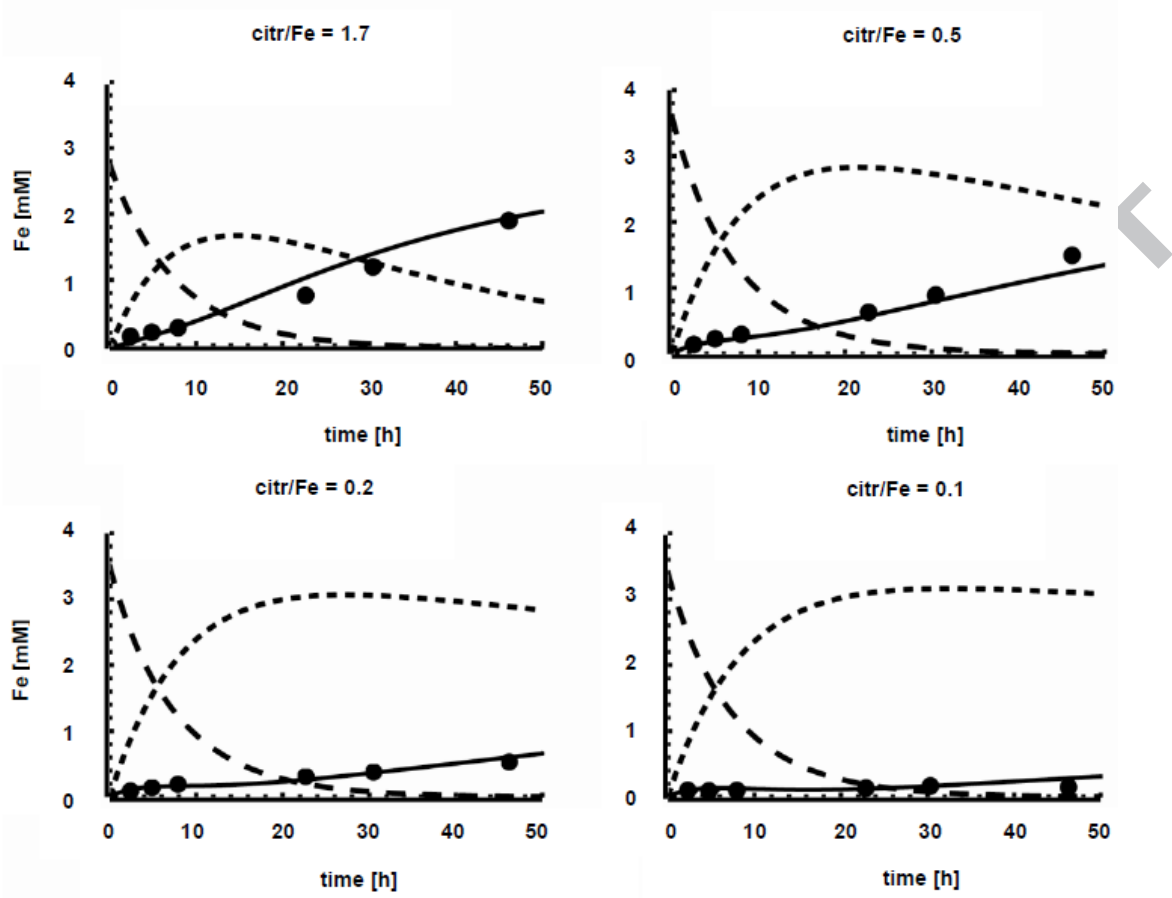

Fig. 4: Modeling results of abiotic ferrihydrite dissolution kinetics at different citr/Fe ratios under formation of ferrihydrite colloids (dashed lines: ferrihydrite aggregates, dotted lines: colloidal ferrihydrite, solid lines: dissolved Fe citrate) and means of measured dissolved Fe citrate (dots).

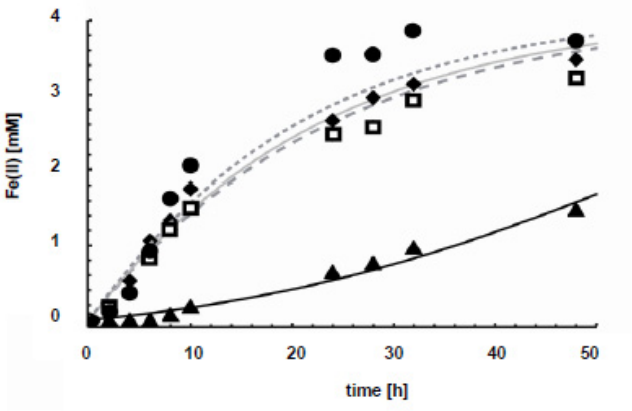

Fig. 5: Modeling results of biotic ferrihydrite reduction kinetics in consideration of ferrihydrite colloid stabilization and ferrihydrite dissolution at different citr/Fe ratios: 0.0 black solid line, 0.14 grey dashed line, 0.27 grey solid line, 0.58 grey dotted line. Symbols show means of measured reduced Fe at different citr/Fe ratios: 0.0 (▲), 0.14 (□), 0.27 (◆), 0.58 (●).

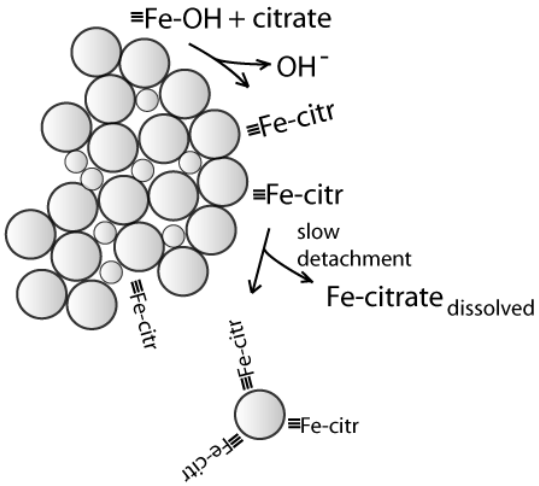

Fig. 6: Schematic illustration of ferrihydrite dissolution and colloid stabilization in the presence of citrate. Citrate dissolves ferrihydrite via ligand exchange. Adsorbed citrate species on ferrihydrite surfaces stabilize single colloids by electrostatic repulsion.

Tables

Tab. 1: Mössbauer hyperfine parameters of ferrihydrite and ferrihydrite incubated with citrate (citrate:Fe = 0.16) at room temperature, 77 K, and ~ 5 K.

	room temperature		77 K			~ 5K		
	δ^1 [mm s^{-1}]	Δ^2 [mm s^{-1}]	δ^1 [mm s^{-1}]	Δ^2 [mm s^{-1}]	$B_{hf}{}^3$ [T]	δ^1 [mm s^{-1}]	Δ^2 [mm s^{-1}]	$B_{hf}{}^3$ [T]
ferrihydrite	0.35	0.74	0.46	0.77		0.46	-0.04	48.8
			0.52	0	9.5			
ferrihydrite + citrate	0.35	0.73	0.46	0.71		0.46	-0.03	48.4

[1] isomeric shift; [2] quadrupole splitting; [3] hyperfine field

Tab. 2: Abiotic dissolution rate constants fitted for all measured dissolution curves under treatment with different citrate additions. k_1 and k_2 are first and second order dissolution rates of ferrihydrite aggregates, k_3 is dissolution rate of colloids.

Dissolution rate constants	k_1	k_2	k_3
SQR fitted values (h^{-1})	0.12	0.006	0.007

Tab. 3: Modeling efficiency (EF) and correlation coefficient (r) for simulation results of dissolution rate (abiotic) and reduction rate kinetics (biotic).

abiotic				
citr/Fe ratio	1.7	0.5	0.2	0.1
EF	0.937	0.958	0.955	-0.600
r	0.988	0.998	0.983	0.847
biotic				
citr/Fe ratio	0.58	0.27	0.14	0.0 (control)
EF	0.936	0.987	0.975	0.973
r	0.983	0.993	0.996	0.987

Tab. 4: Biotic reduction rate constants for ferrihydrite aggregates ($k_{bio,1}$), colloids ($k_{bio,2}$), and Fe-citrate ($k_{bio,3}$) fitted for all measured reduction curves for different citrate additions and the control.

Reduction rate constants	$k_{bio,1}$	$k_{bio,2}$	$k_{bio,3}$
SQR fitted values (h^{-1})	0.011	0.04	0.1